台灣石油地質第三十三期
第21-42頁, 16圖, 民國88年12月

PETROLEUM GEOLOGY OF TAIWAN NO.33
P. 21 ~42, 16 FIGS, DEC. 1999

Constraints on Free Gas and Gas Hydrate Bearing Sediments from Multi-Channel Seismic Data, Offshore Southwestern Taiwan

PHILIPPE SCHNURLE[1], TA-HENG HSIUAN[1], and CHAR-SHINE LIU[2]

ABSTRACT

In this study, we analyze several seismic profiles Offshore southern Taiwan and present the results along 2 perpendicular multi-channel seismic profiles located in the northwestern portion of the Manila accretionary wedge where the highest concentration of BSR is observed. In this area, rapid deposited terrigenous sediments derived mainly from the Chinese continental margin, then accreted, may have relatively high amounts of organic carbon, thereby providing a source for the methane. MCS579-03 runs downslope across the acretionary wedge and shows a prominant BSR. The seismic signature of the sediments above and bellow the BSR varies considerably depending on the water depth and structural context. Seismic whitening is generally observed between the sea-floor and the BSR, while at numerous locations, high amplitude and low frequent reflectors underneath the BSR strongly suggest the presence of free gas within the pore space. MCS367-23 runs in the axis of the upper-slope of the accretionary wedge. In order to providing an assessment of the amount and distribution of free gas and gas hydrates in southwestern Taiwan, we conduct a detailed velocity analysis of the pre-stack time migrated records. Compressional velocity are relatively constant in the strata above the BSR with a mean value of 1880 m/s. Dramatic decrease in the instantaneous interval velocity is mapped within several zones located at and bellow the BSR, that confirms the presence of free gas in the pore space. These results are compared to theoretical elastic properties for the 3-phase matrix of gas hydrates and free gas saturated sediments. Finally, reflection strength and frequency attenuation, gathered in an attribute analysis further constrain our estimates.

INTRODUCTION

Bottom-parallel or Bottom-simulating seismic Reflector (BSR) have widely been observed in various continental margin environments. The BSR is commonly interpreted as marking the base of the stability field for gas hydrate (e.g. Miller et al., 1991; Hyndman and Davis, 1992; Bangs et al., 1993; Dillon et al., 1996). Gas hydrates are christalline solid, formed of a cage of water molecules surrounding a natural gas molecule (low molecular weighted gas, commonly of methane), under specific conditions of relative high pressure and low temperature, when gas concentration exceeds those which can be held in solution (Sloan, 1990). For instance, experimental results of methane hydrate synthesis indicate that hydrates occur in water depth greater than 280 m, when the temperature at sea-level is 0º. The hydrated layer is commonly underlain by strata bearing free methane gas. The effect of strong acoustic impedance contrast between sediments containing gas hydrates and sediments with free gas in the pore-space results in a high amplitude acoustic reflector with negative polarity, the BSR (e.g. Hydman and Spence, 1992; Katzman et al., 1994; Andreassen et al., 1997; Sain et al., 2000).

During the ODP Leg 164 (e.g. Paull et al., 1996; Dickens, et al., 1997; Guerin et al., 1999), on the continental margin off southeastern North America, a study of natural gas hydrates in marine sediments has been conducted. From 200 to 450m bellow sea floor, gas hydrates have been drilled and recovered. During coring, several direct measurements and indirect estimates of the hydrate saturation where conducted. Paull et al. (1996) concluded that, at the three drill sites, the gas hydrates occupy more than 1% of the bulk sediment volume, resulting in 5 to 15 % saturation of the pore space depending on the porosity. Further more, the chemical and isotopic composition of the gases recovered from the core samples all indicate that the gas is primarily microbialy produced via CO2 reduction (Egeberg and Barth, 1998; Egeberg and Dickens, 1999). Traces of ethane and methane, as well as changes in pore water chemistry and isotopic composition of recovered gas, suggest that the majority of methane and dissolved carbon dioxide where not locally produced and migrated from bellow into the system.

Methane stored within and beneath hydrates may provide a major energy resource (Kvenvolden, 1993). Release of methane into the atmosphere is also an important factor in global warming. Further more, hydrates may form a barrier to fluid flow and inhibit sediment consolidation, leading to excess in pore fluid pressure at the BSR (gas hydrate decomposition equally results in excess in pore fluid pressure), that could result in locally reduced shear strength and slope failure (Booth et al., 1994). Free gas trapped beneath hydrated areas is also a significant drilling hazard.

Offshore southern Taiwan, Reed et al. (1992) first recognized the occurrence of a BSR. In 1998, Chi et al. published a comprehensive map of the distribution of BSR in southern Taiwan. These authors examined more than 8,000 km of seismic data and concluded that at least 70,000 km^2 of the Taiwan accretionary prism, in water depths ranging from 500 to 2000 m, is covered by BSRs. The highest concentration of BSR is located in the northwestern part of the studied area, where rapid deposited terrigenous sediments may have relatively high amounts of organic carbon, thereby providing a source for the methane. In this study, we analyze several multi-channel seismic profiles offshore southwestern Taiwan, and examine means to estimate the amounts of gas hydrate and free gas contents in this area.

GEODYNAMIC SETTING

The island of Taiwan is located at the junction of the Ryukyu and Luzon island arcs along the western margin of the Philippine Sea. Complex flipping of the subduction directions exists underneath Taiwan (Figure 1). East of Taiwan, the Philippine Sea plate is being subducted northward underneath the Eurasian plate along the Ryukyu subduction system, while south of Taiwan, the South China Sea is being subducted eastward underneath the Philippine Sea plate along the Manila subduction zone (Karig, 1973; Bowin et al., 1978; Angelier, 1986). The orogen of Taiwan results from the collision of the Luzon volcanic arc with the passive Chinese continental margin since Pliocene time (Biq, 1972; Ho, 1986; Teng, 1990). The obliquity of the convergence, (307º N versus 350-10º trend of the collision zone, at a rate of about 7 cm/yr.; Seno et al., 1993), induces a southward propagation of the collision (Suppe, 1987) from a mature stage along the Coastal Range, the onland portion of the Luzon arc in eastern Taiwan (Ho, 1986), to initiation with the closure of the Luzon forearc basin and thrusting of the Huatung ridge over the Luzon arc (Lundberg et al., 1992; 1997; Hwang et al., 1992; Reed et al., 1992, Malavieille et al., 2000). According to GPS measurements (Yu et al., 1997), while south of 24º, the convergence is almost totally distributed on Taiwan, the mountain building process has apparently ceased in the northern Taiwan (Yu and Chen, 1994), and the northeastern part of Taiwan may have evolved into the extensional Ryukyu back-arc system (Teng, 1995).

South of Taiwan, along the Manila subduction zone, the sediments derived from both the Taiwan orogenic belt as well as the Chinese continental margin deposit in the South China Sea and are subsequently accreted to Manila accretionary prism (Reed et al., 1992). Northward, the Manila subduction system evolves into the Taiwan collision zone. At the latitude of 22º33’, the accretionary wedge terminates against the southeastern edge of the Chinese continental shelf (Yu and Chiang, 1997). In this area, much of the relative convergence between the Chinese continental margin and the Philippine sea plate is taken on-land Taiwan (Yu et al., 1997). Large amounts of terrigenous sediments, mostly derived from the Chinese continental shelf, rapidly deposit in the northern extremity of the south China sea (bathymetric deep), west of Taiwan. The Kaoping canyon, clearly imaged on the bathymetric data (Liu et al., 1993; Figure 2), conducts most sediments eroded from the Taiwan island toward the south, and constitutes a structural boundary for sedimentary input into deep sea basin located westward. An accretionary wedge has developed, aproximativly 80 km wide, that is characterized by defuse deformation and strain partitioning (Reed et al., 1992).

SEISMIC REFLECTION DATA OFFSHORE SOUTHWESTERN TAIWAN

In order to providing an assessment of the amount and distribution of free gas and gas hydrates in southwestern Taiwan, we have conducted, over the last year, a careful analysis of most seismic data available in the area (more than 8,000 km of seismic reflection profiles, over a region of 27,000 km^2; ship tracks are marked on Figure 1). Most of these profiles have been previously studied by Chi et al. (1998). East of the Kaoping canyon, the structures of the accretionary wedge are highly disrupted on available seismic data and no BSR was observed. As a matter of facts, we might assume that the Kaoping canyon constitutes a structural boundary for the occurrence of gas hydrates. Strong multiples make fine analysis more difficult in water depth shallower than 500 m. Thus, in this paper, we analyze 4 unpublished seismic profiles, located to the north of Chi et al's comprehensive map of the distribution of BSR in southern Taiwan, and presenting large sections where a strong BSR is clearly identified in water depth raging from 500 to 3000 m.

M367-21 and M367-23 were acquired by the Institute of Oceanography, National Taiwan University in 1994, on board the R/V Ocean Researcher I, along two NW-SE parallel profiles (Figure 3). The 2 seismic profiles are located at the northern end of the Manila accretionary margin and run approximately in the axis of the prism, with water depths ranging from 100 m to the NW where the accretionary wedge end against the continental shelf, to 1000 m to the SE near the Kaoping Canyon, with maximal water depth of 1,800 m in the center of the profiles. The seismic data was recorded by a 56 channel streamer, 1580 m in length (25 m group spacing). A small air-gun array, with a total volume of 580 l, was fired every 50 m. MCS579-01 and MCS579-03 were acquired by the Institute of Oceanography, National Taiwan University in 2000, on board the R/V Ocean Researcher I. The seismic profiles run NE-SW across the accretionary wedge. Water depths range from 700 m to the NE near the Taiwan shore line, to 2000 m to the SE in the Manila Trench, with a total profile's length of 100 km. The seismic data was recorded by a 24 channel solid streamer, 700 m in length (12,5 m group spacing) with 25 m shot spacing. The seismic sections presented in this study are the center section of MCS367-23 and MCS579-03, where the quality of the data as well as the analysis results are the most relevant for the study of gas hydrates.

A conventional processing sequence was applied to the data and can be described as the following :

Data Acquisition
Editing
Geometry

⇓

Pre-Processing
Start Times & Muting
Spiking Predictive Deconvolution
True Amplitude Recovery
Band Pass Filter

↗ ↘

Pre-Stack Time Migration

⇓

Interactive Velocity Analysis

↘ ↗

Normal Move-out
Stack

⇓

Post-Processing
Post-Stack Time Migration
Attribute Analysis

On the seismic sections presented in this study, a mean gain was applied in order to better scale the decrease in time and strong lateral variations of the amplitudes, so that both relative amplitude and structural analysis can be comprehended together. However, true amplitude stacked sections and attribute analysis were generated for the characterization of reflection strength properties.

Figure 4 presents the seaward portion of seismic profile MCS579-03, in the south China sea and the Manila Trench (see Figure 3 for location). Numerous NW-SE submarine channels flow from the Taiwan banks into the South China Sea and rapidly merge to the NE-SW Penghu Canyon (Figure 1 and 2). The Penghu canyon then follows the NNW-SSE axis of the Manila Trench in water depths of approximately 3000 m (Figure 4). These channels carry important amounts of sediments derived from the chinese continental margin and deposited into the oceanic basin. On the seismic profiles available in this area, the acoustic basement is not located precisely. However, more than 3 s TWT of sediments enter the Manila Trench and are subsequently accreted to Manila accretionary prism, as attested by the sharp deformation front and seaward vergent thrust imaged in the incoming sediments on seismic profile MCS579-03. These terrigenous detritus may have relatively high amounts of organic carbon elements, thereby providing a source for the methane formation.

The lower slope of the accretionary wedge is composed by two accretionary units, 18 and 9 km wide, in water depth of approximately 2000 and 1700 m respectively. The folding of the sedimentary strata is remarkably well imaged in the trenchward anticline. On the seismic section, 350 to 500 ms Twt bellow the sea-floor, the BSR is easily recognized because it presents a reversed polarity reflection, consistent with a negative acoustic impedance due to the drop of acoustic velocities

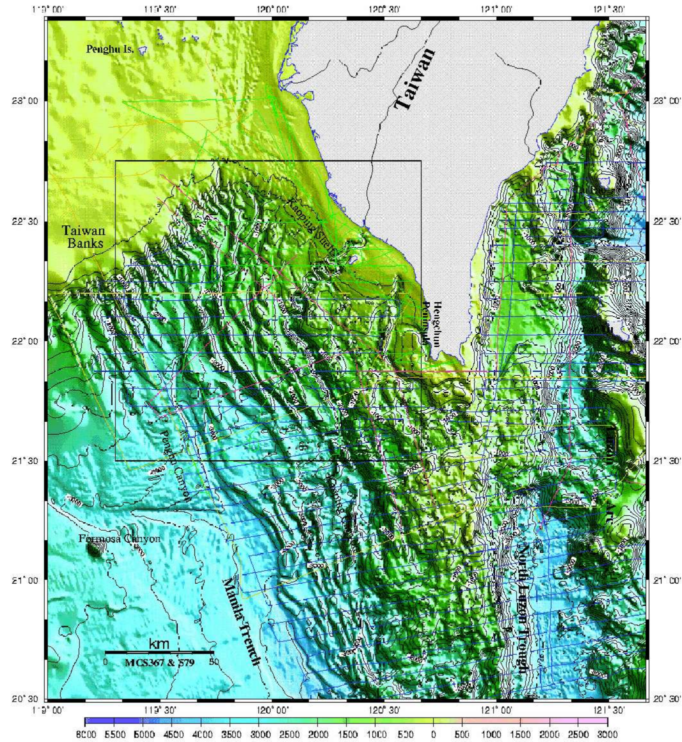

Figure 1: Bathymetric shaded image of southwestern Taiwan (after Liu et al., 1998). The studied area is marked by a box corresponding to Figure 2 (seismic profile location map). Contours are every 200 m. Ship tracks for geophysical cruises conducted in this area are overlain.

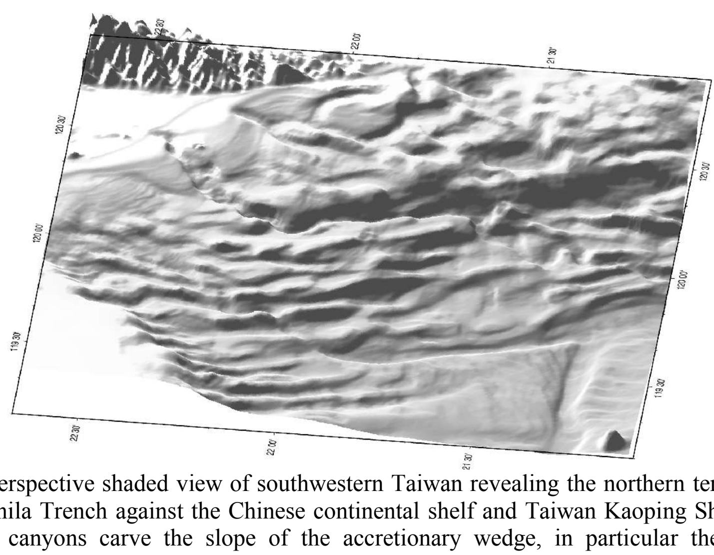

Figure 2: 3D perspective shaded view of southwestern Taiwan revealing the northern termination of the Manila Trench against the Chinese continental shelf and Taiwan Kaoping Shelf. Several erosive canyons carve the slope of the accretionary wedge, in particular the prominent Kaoping Canyon.

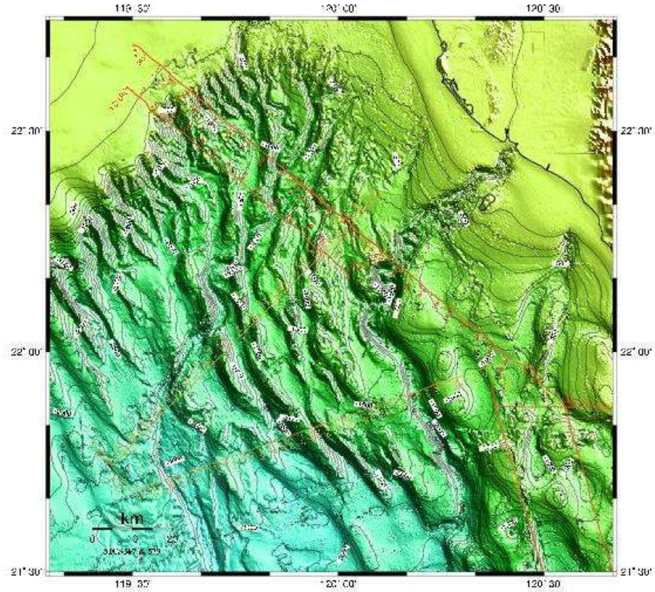

Figure 3: Location map of seismic profiles MCS367-21, MCS367-23, MCS579-01, and MCS579-03. Sections presented in this study are marked in black The bathymetric data is shaded from the NE and contoured every 100 m. Shot numbers are annotated.

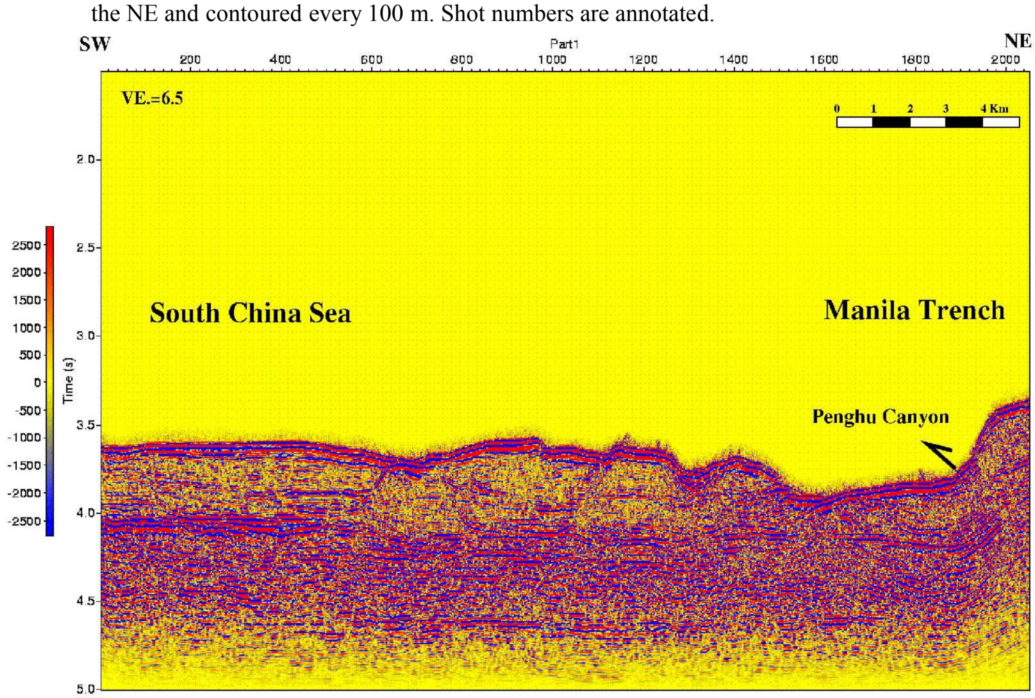

Figure 4: Seaward portion of seismic profile MCS579-03, post-stack time migrated.

from water-gas hydrate to water-free gas bearing sediments. The BSR is best recognized when the reflector cross-cuts the dipping sedimentary strata. The BSR is gently parallel to the sea-floor but its curvature is generally smaller than that of the sea-floor. Few reflector are imaged above the BSR. This whitening effect may be related to the presence of gas hydrates distributed within the overlaying stratigraphy. The amplitude of the BSR varies considerably depending on the water depth and structural context. However, the refection strength of the reflector commonly approaches that of the sea-floor reflection. At structural deeps, in the rear of the anticlines associated to the accreted units, high amplitude and low frequent reflectors underneath the BSR strongly suggest the presence of free gas.

Structures within the accretionary wedge become very complex in the middle slope. Three major tectonic units, 10 to 12 km wide, are accreted against the southwestern slope of the Kaoping Shelf, in water depth of approximately 1300 to 1500 m (Figure 6). As a matter of facts, the obliquity of the convergence and the proximity of the Chinese continental shelf to the north are inducing stain partitioning: considerable N-S shortening superimpose on the E-W accretionary folding, as attested by the perpendicular seismic profile MCS367-23 presented in the next section (Figure 3). However, the BSR is clearly imaged along several portions of the middle slope and can be followed over the entire section with large variations in reflection strength. The BSR presents similar characteristics as in the lower slope. Furthermore, seismic whitening is generally observed between the sea-floor and the BSR.

A structural high marks the transition from the accretionary wedge to the Kaoping Shelf in the upper slope of seismic profile MCS579-03. This ridge is also imaged on seismic profile MCS367-23. According to the seismic signature of the strata composing the ridge, it is formed by a fold in the consolidated Kaoping Shelf basement. From the bathymetric data, this ridge extends only slightly northward and south-eastward for approximately 30 km, in water depth shallower than 1000 m, and could relate to the turn in the path of the Kaoping Canyon from a NE-SW down slope path to a NW-SE path. The top of this consolidated strata can be followed eastward on the seismic profile (Figure 7). In the center of Figure 7, a mud diapir is imaged. In the southwestern portion of the upper slope, a strong BSR (with negative polarity) is recognized cross cutting the stratigraphy. This reflector is better imaged in the multiple where the relative reflection strength of the sea-floor is attenuated. Toward the end of seismic profile MCS579-03, it is difficult to acess the presence of a BSR.

The southeastern portion of MCS367-23 intersects MCS579-03 near the structural high (Figure 3 and 8). The BSR is poorly observed on the steep slopes of the ridge, then more clearly on either sides according to its reversed polarity when compared to the bedding reflectors. Seismic whitening is predominant above the BSR. Fortunately, between CMP 2850 and 2975 for instance, coherent reflection are observed. These reflector can be used to determine the acoustic velocities above the BSR that can not be determined else where in poorly reflective stratigraphy. In the central of this profile (Figure 9), due to strain partitioning, considerable NNW-SSE

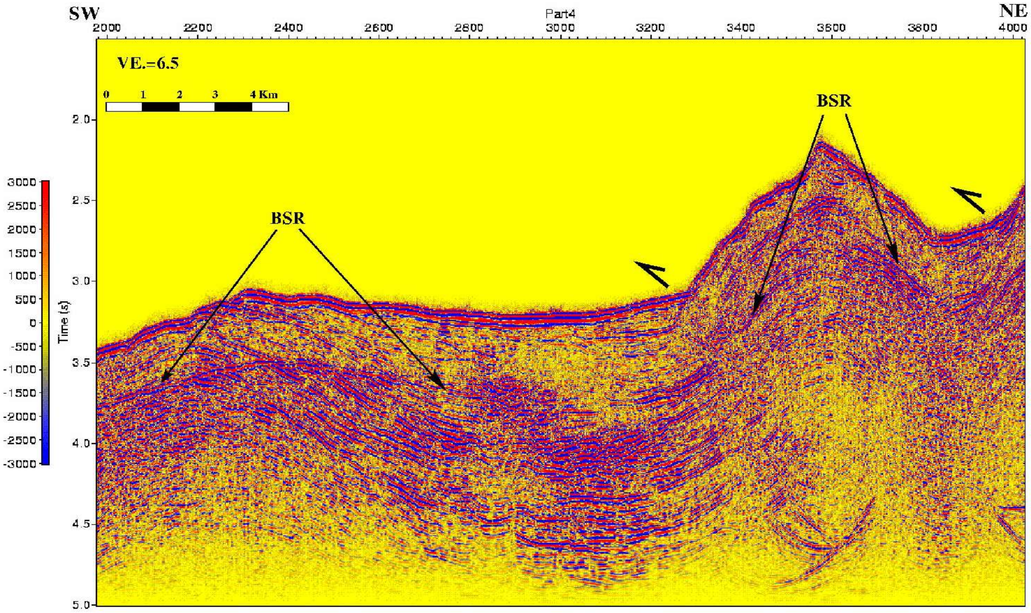

Figure 5: Lower slope portion of seismic profile MCS579-03, post-stack time migrated.

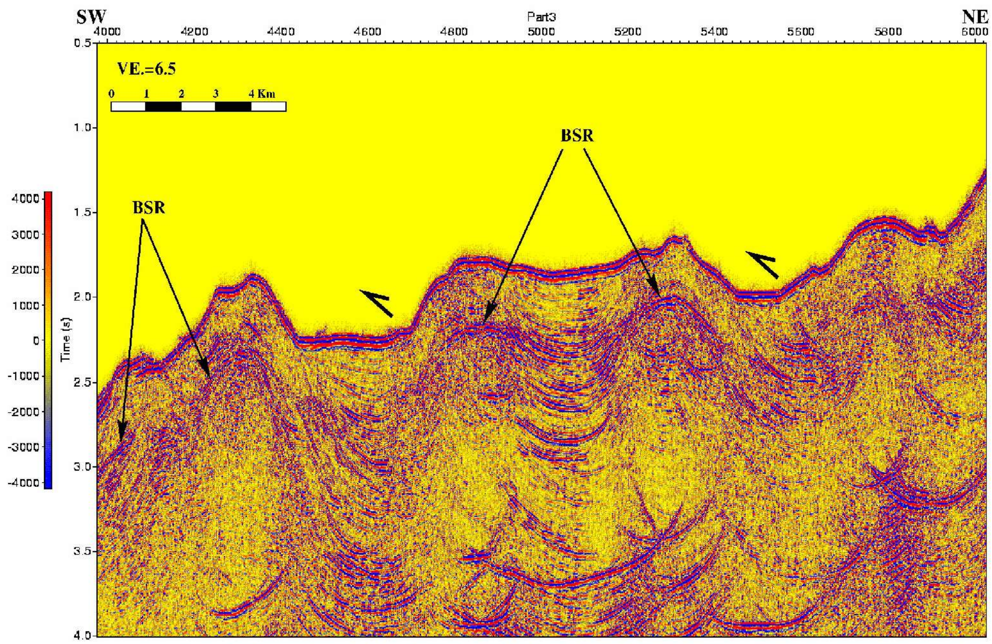

Figure 6: Middle slope portion of seismic profile MCS579-03, post-stack time migrated.

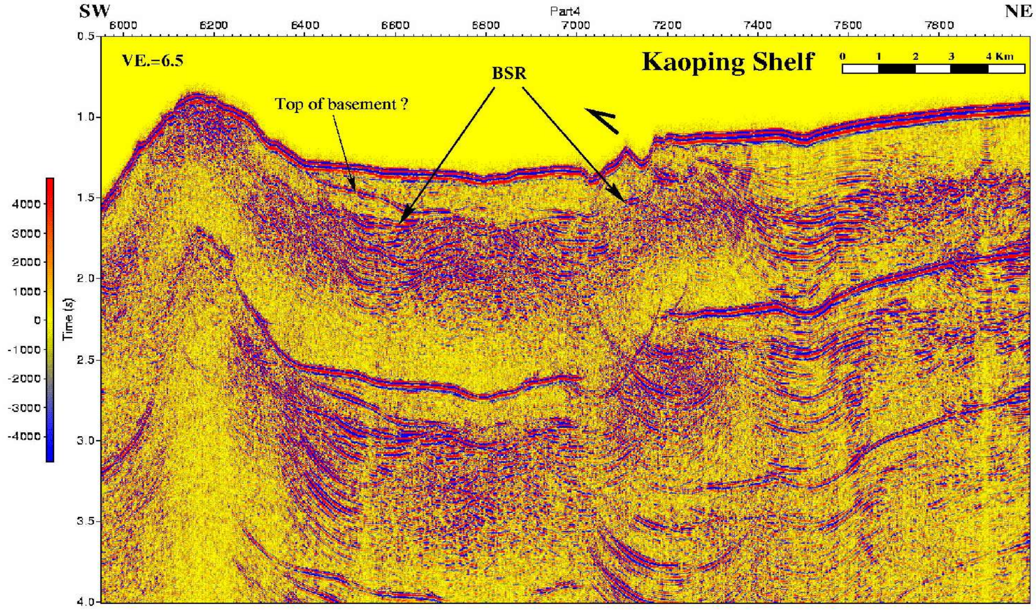

Figure 7: Upper slope portion of seismic profile MCS579-03, post-stack time migrated.

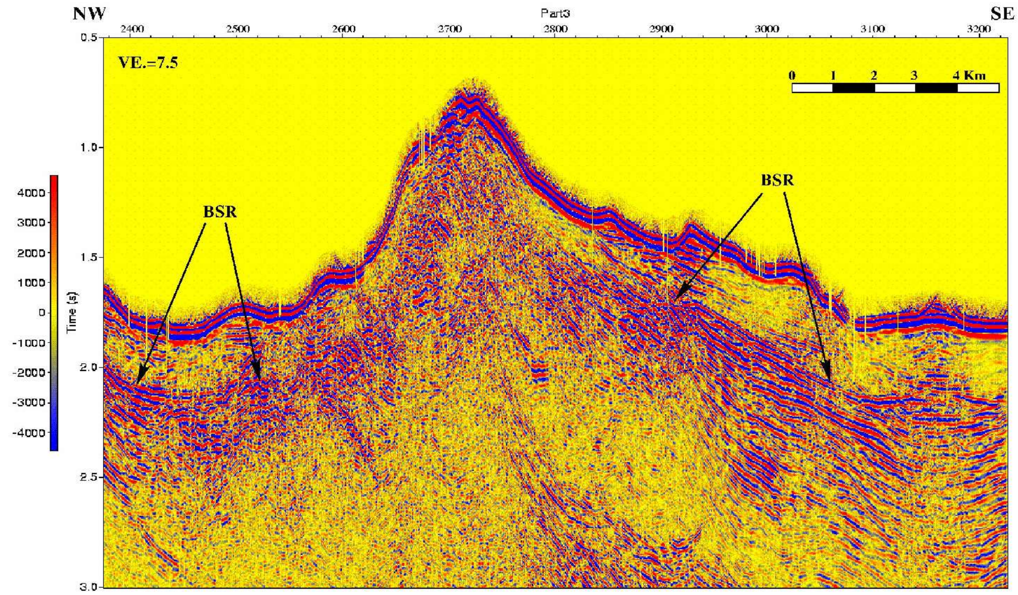

Figure 8: Southeast portion of seismic profile MCS367-23, post-stack time migrated.

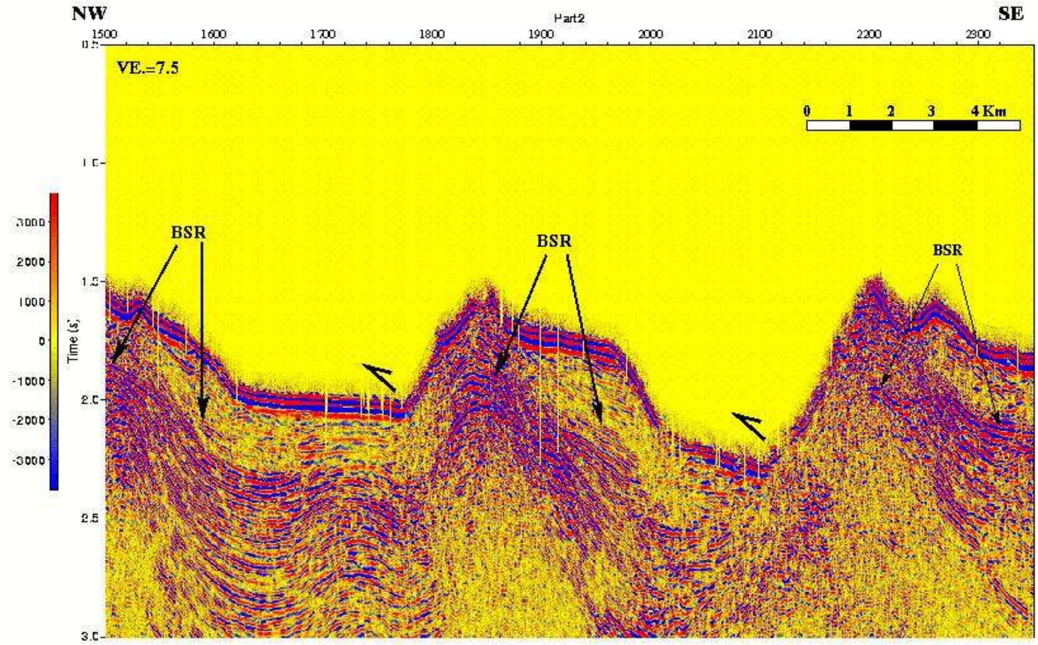

Figure 9: Central portion of seismic profile MCS367-23, post-stack time migrated.

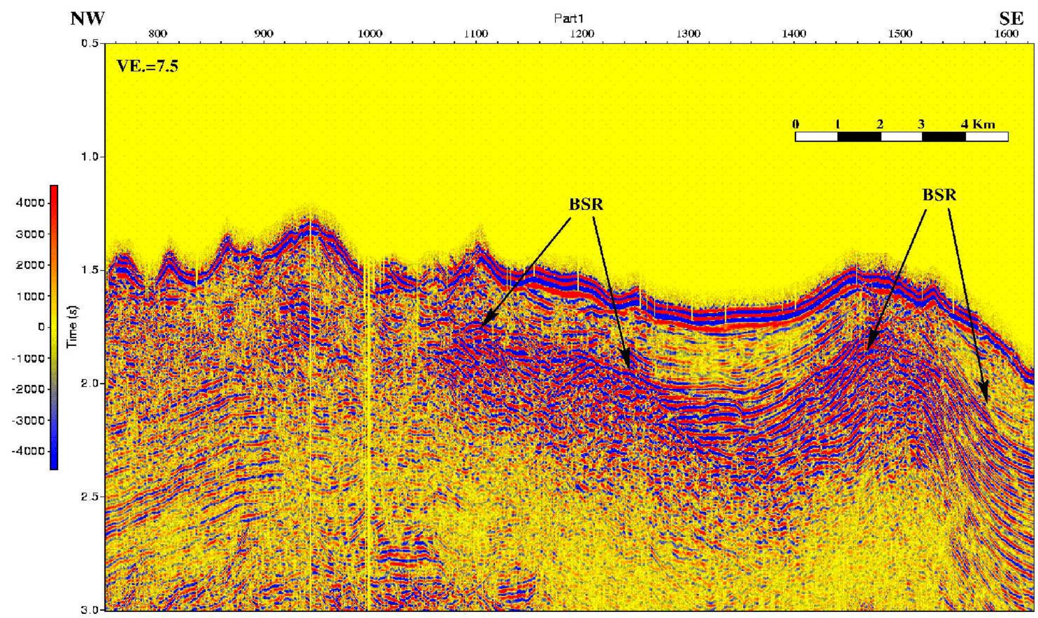

Figure 10: Northwest portion of seismic profile MCS367-23, post-stack time migrated.

shortening occurs perpendicular to the slope of the accretionary wedge. Further more, the sea-floor is incised by 2 erosive channels located between the anticlines on MCS367-23. As approaching the transition to the Taiwan Banks in the NW, submarine channels become narrower and more numerous. The rough topography degrades the seismic image and locating the BSR is compromised. The reflection strength of the BSR is highly variable, and systematically increases at the crest of the anticlines, where the bedding presents steep dips, while decreasing in flat bedded areas.

BSR SUB-BOTTOM DEPTH AND THERMAL GRADIENT

Laboratory synthesis of methane hydrates (Sloan, 1998) show that gas hydrates are stable in a pressure versus temperature stability zone (Figure 11). Lithostatic pressure (e.g. Trehu et al., 1995; Ganguly et al., 2000) or hydrostatic pressure (e.g. Hyndman et al., 1993) at the depth of the BSR can be computed when the porosity and density of the sediments are known. Often empirical relations, such porosity versus compressional velocity (Hamilton, 1976; 1980), are used to compensate for the absence of in-situ measurements. Based on the sub-bottom depth of the BSR and a set of superficial measurements of the thermal gradient, and assuming a constant pressure gradient from the sea floor to the depth of the BSR, Shyu et al. (1998) as well as Chi et al. (1998) propose estimates of the thermal gradient in the Taiwan offshore area. These authors conclude in large variability of geothermal gradients, ranging from 17 to 160º/km with most of the values around 25-45 º/km.

Since accurate interval velocities are not available for MCS579-03, the two-way travel time to the BSR from the seismic profiles is converted to sub-bottom depth (Figure 12) following a single formula derived from a data set of samples drilled at active margins (Hamilton, 1980):

Mbsf=1511 x t + 1041 x t^2 – 372 x t^3, where t is the two-way travel time to BSR.

For a given composition of gas and water, a temperature at the each pick can be proposed. Geothermal values estimated from BSR sub-bottom depth are strongly dependent on this gas composition, which remains unknown until some sample of hydrates are recovered in this area. The scatter in the data results mainly from picks at similar water depths but different geographical locations, that confirm variations in the geothermal gradient in the surveyed area. Further more, picks in water depth greater than 2700 m on MCS579-03 (and marked with light dots on Figure 12) correspond to a reflector in the sedimentary sequence on the South China Sea that is not associated with gas hydrates. These picks clearly deviate from the stability behavior, and show the ability to discriminate events that are mistaken for a BSR, such as an unconformity for example.

Figure 11: Depth (assuming a 5.795 kPa/m pressure gradient) versus Temperature stability curve for

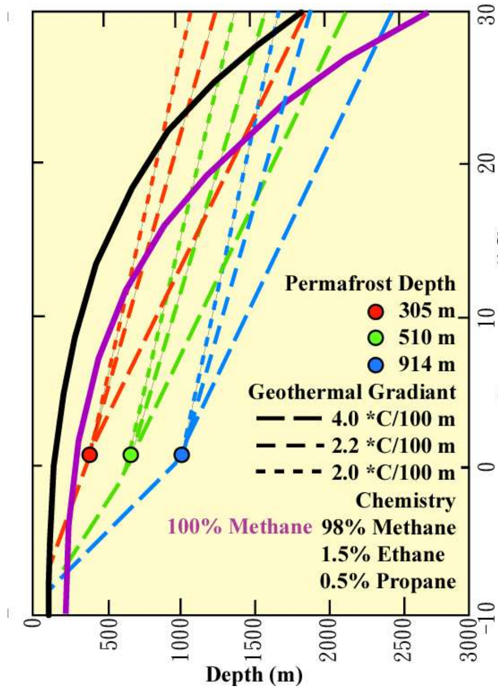

methane hydrate in permafrost regions.

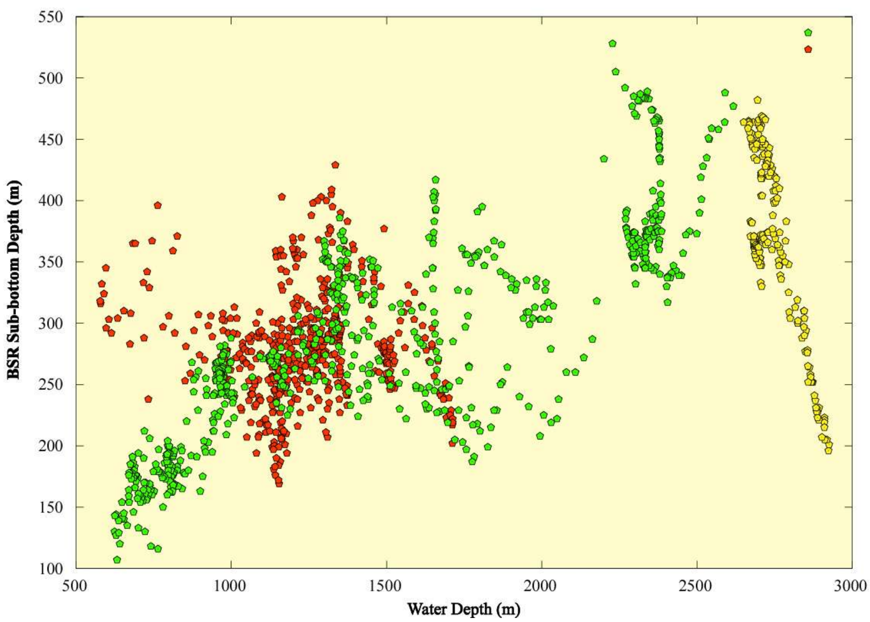

Figure 12: BSR sub-bottom depth versus water depth along MCS367-23 and MCS579-03.

ACOUSTIC PROPERTIES OF HYDRATE AND FREE GAS

BEARING SEDIMENTS

Information about velocities are indispensable in areas where direct measurements are not available to characterize the presence of gas hydrate bearing layers and/or free gas bearing layers. Laboratory measurements of pure methane hydrate density and acoustic velocity range respectively from 1.024 to 1.045 g/cm3 and 3.3 to 3.8 km/s (Sloan, 1990). The combination yield a moderate acoustic impedance contrast from that of surrounding sediments, suggesting a small reflection coefficient at normal incidence, although a large compressional velocity contrast produces a larger reflection at larger angles of incidence (e.g. Singh et al., 1993; Singh and Minshull, 1994; Wood et al., 1994). Further more, small quantities of gas in the pore space of marine sediments cause a dramatic decrease in compressional velocity, while further increase cause little change (Figure 13). Shear wave velocity slightly increase with increasing gas saturation, with its maximum variation near full saturation (Minshull et al., 1994; Tinivella and Accaino, 2000). Therefore, the BSR is mainly caused by the reflection across the interface between hydrate bearing and gas saturated sediments. Thus, the same amount of gas hydrates was proposed at the sites 994, 995, and 997 (ODP Leg 164, e.g. Paull et al., 1996) although no BSR is imaged at the vicinity of site 994.

Reflection strength depends on the contrast of seismic impedance (i.e. velocity multiplied by density). On one hand, only a few percent of free gas in the pore space of sediments decreases the compressional velocity drastically (Domenico, 1976; 1977). Therefore layers that contain free gas often generate strong reflections (bright spots). Free gas is also know to highly attenuate acoustic waves. The amplitude decrease depends on the number of wave cycles along its path. For a particular region of high attenuation, shorter wave length (i.e. high frequency) energy will be preferentially attenuated (Taylor et al., 2000). The result is a shift towards lower frequencies of reflection arrivals from below the region of attenuation.

On the other hand, reflections from within the shallow strata are characterized by low amplitude and high frequency seismic signature. Hydrate bearing sediments are often associated to acoustically transparent zone (whitening effect), and together with little seismic attenuation. The increase in compressional velocity depends not only on the saturation of hydrates in the pore space but also on the microscopic distribution of the hydrates in the pore space (e.g. Dvorkin and Nur, 1993; Lee et al., 1996). Various models have been proposed, leading to large variations in theoretical dependence of compressional velocity with respect to hydrate saturation (Figure 14). Disseminated nodules or veins of gas hydrates will accentuate the high frequency and low reflection strength of the seismic signature in the stratigraphy.

Hilbert transform is commonly used to generate seismic attributes such as reflection strength and instantaneous frequency (Taner et al., 1979). In order to combine frequency and reflection strength (as well as attenuation) characteristics, we compute an attribute representing the reflection strength divided by the absolute difference between the instantaneous frequency and the central frequency of the sour-

Figure 13: Variations of seismic velocities and Poisson's ration in ocean bottom sediments at typical

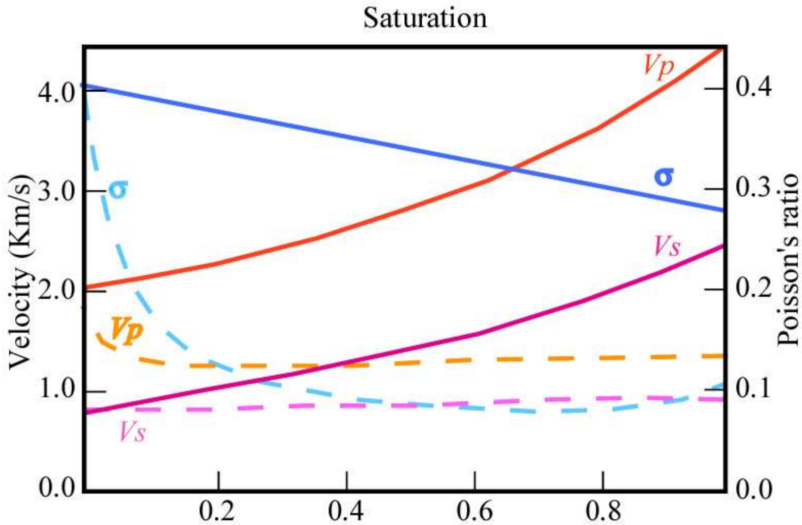

BSR depths (porosity is 0,4) with free gas saturation (dashed lines) and hydrate saturation (solid lines); After Minshull et al., 1994.

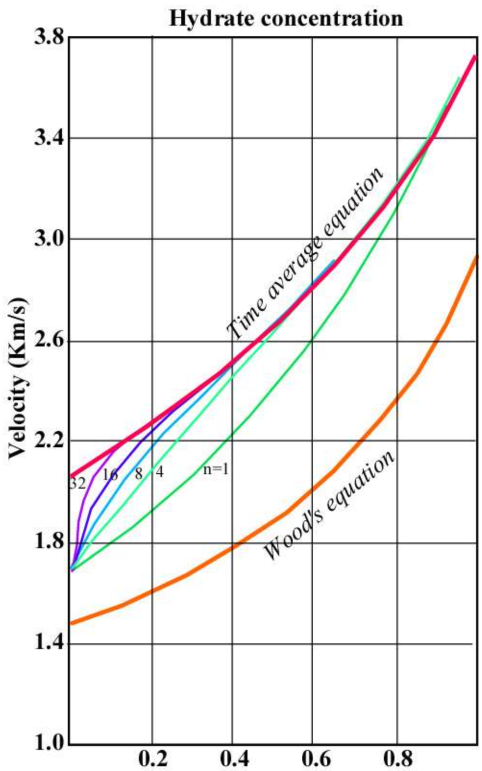

Figure 14: Depth (Pressure) versus Temperature stability curve for methane hydrate in permafrost regions (assuming a 5.795 kPa/m pressure gradient).

ce wavelet.

Finally, in order to further analyze the acoustic properties of the gas hydrate and free gas bearing sediments, we performed a detailed velocity analysis on MCS367-23 seismic records. A series of pre-stack time migration followed by velocity analysis where operated in order to optimize the dip independent velocities. Given the geometry of acquisition, 28 common offset gathers were formed and filtered with a 30Hz high cut frequency to avoid spatial aliasing, then Kirckoff pre-stack time migrated. Conventional stacking velocity analysis was run at 1 km spacing with 5 adjacent CMP in order to increase the signal to noise ratio, resulting in total of 96 analysis location (Figure 15). Then, 4 horizons (sea-floor, reflector above the BSR, BSR, and reflector underneath the BSR) have been used in an automatic velocity picking scheme based on maximal semblance at each CMP. The deviation from the manual picks seldom exceeds 5% (mostly along the reflector in the whitening zone above the BSR, where few coherent reflection occur), and ensures the reliability of the manual picks. The final RMS model was converted to instantaneous interval velocities and is shown in Figure 15, combined with the attribute display.

Since the seismic profile is running in the axis of the accretionary, and in relatively constant water depths, lateral variations of the compressional velocities are expected to be small in the absence or homogeneous distribution of gas hydrates. At most analysis locations, instantaneous velocities are almost constant in the strata above the BSR (Figure 15). Further more, lateral variation is also poor: the average interval velocity in this strata (in a window defined from 60 ms bellow the sea-floor to 60 ms above the BSR) ranges from 1730 m/s (in the northwestern portion of MCS367-23) to 1970 m/s (in the central and southeastern parts), but generally remains near 1880 m/s (Figure 16). The uncertainty over the velocities is however very large. FX pre-stack depth migration of the shot gathers of MCS367-23 has been recently implemented and the depth focusing analysis of the events above the BSR reveals localized deviation from our conventional velocity analysis. In this shallow strata, the reflection strength is generally small. Therefore, the distribution of gas hydrates appears to be rather homogeneous along the strike of this profile. However, the influence of hydrate saturation on the compressional velocity is highly dependent on the porosity of the sedimentary strata which is not constrained in our model. Thus, many unknown ponder an estimate of gas hydrate saturation along MCS367-23.

Numerous areas of strong velocity pull down are mapped. These low velocity zones can be associated to free gas bearing sediments underneath the BGHS (base of the gas hydrates). Their thickness reaches up to 250 ms TwT (Figures 15 and 16). However, a small amount of free gas in the pore space is sufficient to produce the observed velocity pull down. We observe a good correlation in the spatial distribution of anomalies in the attribute and interval velocity models. The largest anomalies in the attribute display concentrate just underneath the BSR, but are some time also observed up to 350 ms TwT below. As a matter of facts, the bright spots in the attribute display are more localized and may therefore be a better indicator of larger free gas saturation.

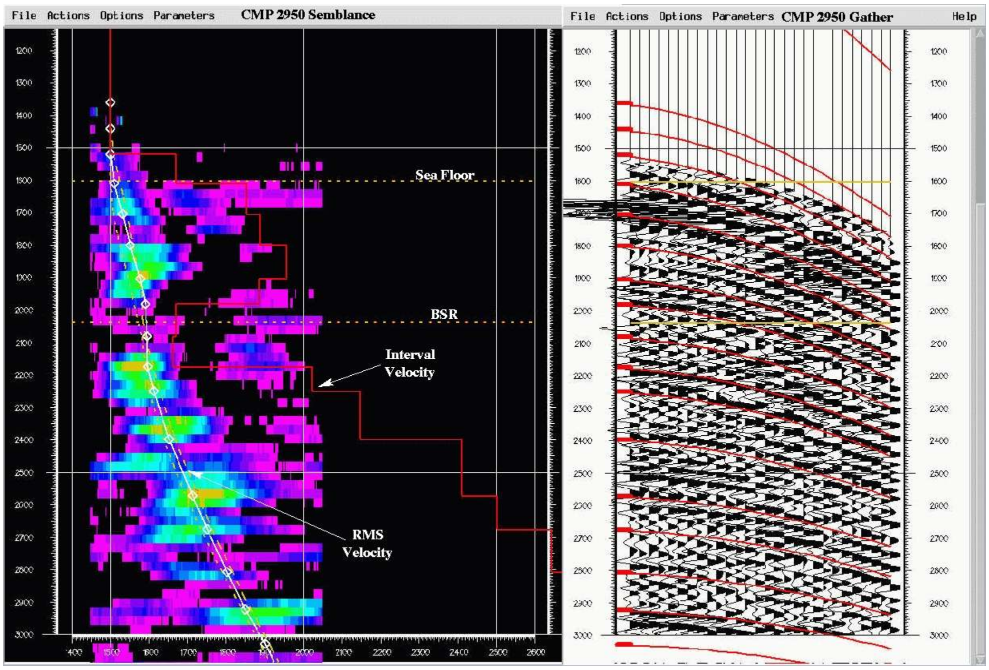

Figure 15: Results from conventional stacking velocity analysis at CMP2975.

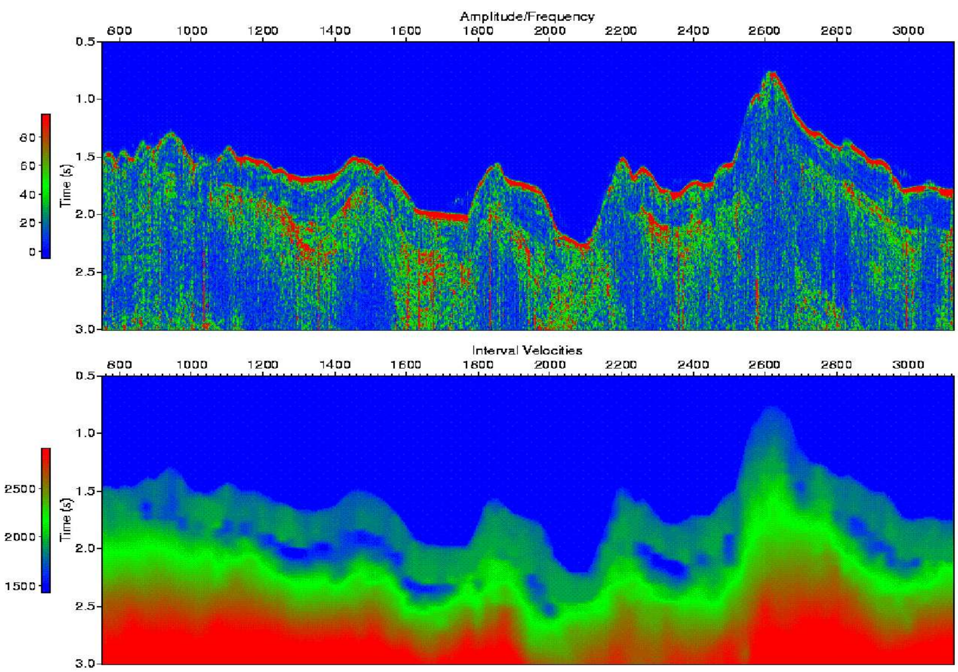

Figure 16: Attribute analysis and instantaneous interval velocity in seismic profile MCS367-23.

CONCLUSIONS

Seismic reflection data is an important key to the characterization of free gas and gas hydrates content offshore southwestern Taiwan. In the seismic profiles presented in this study, the BSR is most commonly found in the crest of anticlines, near mud diapirs, and the vicinity of thrusts. Conventional velocity analysis is well suited to reveal strata bearing free gas in the pore-space. Few coherent reflectors within the hydrated zones allow constrain on the hydrate saturation in this area. Automatic picking along 4 characteristic horizons has proven to be equally efficient, resulting in more dense velocity models and faster processing rate in the future. Reflection strength and instantaneous frequency can be combined into a single attribute that singularizes hydrate bearing sediments (associated with low reflection strength and high frequency seismic signature) and free gas bearing sediments (associated with low reflection strength and high frequency seismic signature) from the background reflections. At this stage, this study remains mostly qualitative. In order to estimate more accurately the amount (or relative amount) of gas hydrates and free gas offshore southwestern Taiwan, we must find means to better characterize the in-situ properties of the sediments of the South China Sea and the Manila accretionary wedge. Combined reflection and refraction seismic experiments prove to be appropriated (e.g. Tinivella and Accaino, 2000). The horizontal component of OBSs (in particular of the converted reflected P waves at the BSR, and the converted transmitted S wave at the BSR and then reflect at the base of the free gas zone) allow to constrain shear wave velocity and Poisson ratio that are valuable for performing more accurately AVO analysis and seismic waveform inversion. Once such qualitative analysis are available, a better understanding in terms of seismic characteristics of formation can be obtained. We will then be able to accurately discuss the importance of structural controls, such as high angle faults, for the vertical transport of the pore water and gas in the concentration of methane hydrates.

ACKNOWLEDGMENTS

We would like to thank the Captains and crews of the R/V Mona Wave and R/V Ocean Researcher I for their efforts in collecting the swath bathymetric and seismic data used in this study. We are grateful to the National Center for Ocean Research and particularly to S.Y. Liu for providing the bathymetric data. Discussions with S.C. Fuh and C.-H. Fan at the CPC-EDRI have help improving our understanding of hydrate and free gas in marine sediments. Maps were generated with GMT (Wessel and Smith, 1995).

REFERENCES

Andeassen, K., P.E. Hart, and A. Grantz, Seismic studies of a bottom simulating reflector related to gas hydrate beneath the continental margin of the Beaufort Sea. J. Geophys. Res., 100, 12659-12673, 1995.

Angelier, J., Geodynamics of the Eurasia-Philippine Sea plate boundary : Preface. Tectonophysics, 125, 1-33, IX-X, 1986.

Bangs L.N.B., C.S. Sawyer, and T. Golovchenko. Free gas at the base of the gas hydrate zone in the vicinity of the Chile triple junction, Geology, 21, 905-908, 1993.

Biq, C.C., Dual-trench structure in the Taiwan-Luzon region. Proc. Geol. Soc. China, 15, 65-75, 1972.

Bowin, C., R.S. Lu, C.S. Lee, and H. Shouten, Plate convergence and accretion in the Taiwan-Luzon region, Am. Assoc. Petrol. Geol. Bull., 62, 1645-1672, 1978.

Chi, W.C., D.L. Reed, C.S. Liu, and N. Lunberg, Distribution of the Bottom Simulating Reflector in the Offshore Taiwan Collision Zone, TAO, 9, 779-793, **1998.**

Dickens, G.R., C.K. Paull, P. Wallace and the ODP Leg 164 scientific Party, Direct measurements of in situ methane quantities in a large gas-hydrate reservoire, Nature, 385, 426-428, 1997.

Dillon, W.P., D.R. Hutchinson and R.M. Dury, Seismic reflection profiles of the Blake Ridge near sites 994, 995, and 997, Proc., Ocean Drill. Program, Init. Rep., 164, 47-56, 1996.

Domenico, S.N., Effects of water saturation on seismic reflectivity of sand reservoir encased in shale: Geophysics, 39, 759-769, 1974.

Domenico, S.N., Effects of brine-gas mixture on velocity in an unconsolidated sand reservoir: Geophysics, 41, 759-769, 1976.

Domenico, S.N., Elasitc properties of unconsolidated porous sand reservoir, Geophysics, 42, 1339-1368, 1977.

Dvorkin, J, and A. Nur., Rock physics for the charaterization of gas hydrates, The Future of Energy Gases. USGS Prof. Paper, 1570, 293-298, 1993.

Egeberg, P.K., and T. Barth, Contribution of dissolved organic species to the carbon and energy budjets of hydrate bearing deep sea sediments (ODP site 997 Balke Ridge), Chem. Geol., 149, 25-35, 1998

Egeberg, P.K., and G.R. Dickens, Thermodynamics and pore water halogen constraints on gas hydrate distribution at ODP site 997 (Balke Ridge), Chem. Geol., 153, 53-79, 1999

Ganguly, N, G.D. spence, N.R. Chapman., and R.D. Hyndman, Heat flow variations from bottom simulating reflectors on the Cascadia margin, Marine Geology, 164, 53-68, 2000.

Guerin, G., D. Goldberg and A. Meltser, Characterization of in situ elastic properties of gas hydrate-bearing sediments on the Blake Ridge, J.G.R., 104, 17,781-17,795, 1999

Hamilton E.L., Variations of density and porosity with depth in deep-sea sediments, J. sediment. Petrol., 46, 280-300, 1978.

Hamilton E.L., Geoacoustic modeling of the sea-floor, J. Acoust. Soc. Amer., 68, 1313-1340, 1980.

Ho, C.-S., A synthesis of the geologic evolution of Taiwan. Tectonophysics, 125, 1-26, 1986.

Hwang Y.L., Geological structural analysis offshore southwestern Taiwan, Master Thesis, Institute of Oceanography, National Taiwan University, pp.1-56, in chinese, 1993.

Hyndman, R.D., and G.D. Spence, A seismic study of methane hydrate marine bottom simulating reflectors, J.G.R., 97, 6683-6689, 1992.

Hyndman, R.D., and E.E. Davis, A mechanism for formation of methane hydrate and seafloor bottom simulating reflectors by vertical fluid expulsion, J.G.R., 97, 7025-7041, 1992.

Karig, D.E., Plate convergence between the Philippines and the Ryukyu islands. Mar. Geol., 14, 153-168, 1973.

Kvenvolden, K.A., Gas hydrate. Geological perpective and global change. Rev. Geophys., 31, 173-187, 1993.

Lee, M.W., D.,R. Hutchinson, T.S. Collet, and W.P. Dillon, Seismic velocities for hydrate-bearing sediments from weighted equation, J.G.R., 101, 20,347-20,358, 1996.

Liu, C.S., N. Lundberg, D.L. Reed, and Y.L. Huang, Morphological and seismic characteristics of the Kaoping Submarine Canyon. Mar. Geol., 111, 93-108, 1993.

Liu, C.S., S.Y. Liu, S.E. Lallemand, N. Lunberg, and D.L. Reed, Digital elevation Model Offshore Taiwan and its tectonic implications, TAO, 9, 705-738, 1998.

Lundberg, N., D. Reed, C.S. Liu, and J. Liekes, Structural controls on orogenic sedimentation, submarine Taiwan collision. Acta Geologica Taiwanica, 30, 131-140, 1992.

Lundberg, N., D. Reed, C.S. Liu, and J. Liekes, Forearc-basin closure and arc accretion in the submarine suture zone south Taiwan. Special issue of Tectonophysics on Active Collision in Taiwan, 274, 1/3, 5-24, 1997.

Malavieille, J., Lallemand, S.E., Dominguez, S., Deschamps, A., Lu, C.-Y., Liu, C.-S., Schnule, P. and the ACT scientific crew. Geology of the arc-continent collision in Taiwan: Marine observations and geodynamic model. Geol. Soc. Am. Spec., in press, 2000.

Miller, J.J., M.W. Lee, and R. von Huene, An analysis of a seismic reflection from the base of a gas hydrate zone, offshore Peru. AAPGB, 75, 910-924, 1991.

Minschull T., and S.C. Singh, Velocity structure of a gas hydrate reflector offshore werstern Colombia, from full waveform inversion, J.G.R., 99, 4715-4734, 1994.

Paull, C.K. et al., Proceding of the Ocean Drilling Program, Initial Report, 164, Colledge Station, Tex., 1996.

Paull, C.K., W.M. Usseler and W.S. Borowski, Methan rich plumes on the Carolina continental rise: Associations with gas hydrates. Geology, 23, 89-92, 1995.

Reed, D.L., N. Lundberg, C.S. Liu, and B.Y. Kuo, Structural relations along the margin of the offshore Taiwan accretionary wedge: implication for accretion and crustal kinematics, Acta Geologica Taiwanica, 30, 105-122, 1992.

Sain, K., T.A. Minschull, S.C Singh.,and R.W Hobbs A E., Evidence for a thick free gas layer beneath the bootom simulating reflector in the Makran accretionary prism. Marine, Geology, 164, 3-12, 2000.

Seno, T., S Stein., and A.E. Gripp, A model for the motion of the Philippine Sea Plate with NUVEL-1 and Geological data. J., Geophys. Res., 9, 17941-17948, 1993.

Shyu, C.-T., S.-K. Hsu, and C.-S. Liu, Heat flows off southwest Taiwan: Measurements over Mud Diapirs and estimates from bottom simulating reflectors, TAO, 9, 4, 795-812, 1998.

Singh, S.C., T.A. Minschull, and G.D. Spence, Velocity structure of a gas hydrate reflector, Science, 260, 204-207, 1993.

Singh, S.C., and T. Minschull, Velocity structure of a gas hydrate reflector at Ocean Drilling program site 889 from a global seismic waveform inversion, J.G.R., 99, 24,221-24,233, 1994.

Sloan, E.D., Clatherates Hydrates of Natural Gases, Marcel Decker, New York, pp. 1-641, 1990.

Sloan, E.D., Clatherates Hydrates of Natural Gases, Marcel Decker, New York, pp. 1-641, 1998.

Suppe, J., The active Taiwan mountain belt. In: J.P. Schaer and J. Rodgers (Editors), Comparative Anatomy of Mountain Ranges, Princeton University Press, 277-293, 1987.

Taner, M.T., F. Koehler, and R.E. Sheriff, Complex trace analysis, Geophysics, 44 (6), 1041-1063, 1979.

Taylor, M.H., W.P. Dillon, and I.A. Pecher, Trapping and migration of methane associated with the gas hydrate stability zone at the Blake Ridge Diapir: mew insight from seismic data, Marine Geology, 164, 79-89, 2000.

Teng, L.-S., Geotectonique evolution of the late Cenozoic arc-continent colision in Taiwan. Tectonophysics, 183, 57-76, 1990.

Teng, L.S., Neotectonics of northern Taiwan and southern Ryukyu. In: Sino-French Symposium on Active Colision in Taiwan, Taiwan, 287-292, 1995.

Tinavella, U., and F. Accaino, Compressional velocity and Poisson's ratio in marine sediments with gas hydrate and free gas by inversion of reflected and refracted seismic data (South Shetland Island, Antartica), Marine Geology, 164, 13-27, 2000.

Trehu, A.M, G. Lin, E. Maxwell, and C. Goldfinger, A seismic reflection profile across the Cascadia subduction zone offshore central Oregon: new constraints on methane distribution and crustal structures, J. Geophys. Res., 100, 15,101-15,116, 1995.

Wessel, P., and W.H.F. Smith, new version of the Generic Mapping Tools released, Eos Trans., AGU, Suppl., 76, 17, 329, 1995.

Wood, A.B., A text book of sound, Macmillian, New York, 578pp, 1941.

Wood, W.T., P.L. Stoffa, and T.H. Shipley, Quantitative detection of methane trough high resolution seismic velocity analysis, J.G.R., 99, 9681-9695, 1994.

Yu, H.S. and C.S., Chiang, Kaoping Shelf: morphology and tectonic significance; Journal of southeast Asian Earth Sci., 15, 1, 9-18, 1997.

Yu, S.B., H.Y. Chen, and L.C. Kuo, Velocity field of GPS stations in the Taiwan area. Special issue of Tectonophysics on Active Collision in Taiwan, 274,1/3, 41-59, 1997.

台灣西南海域甲烷水合物震測研究

史菲利 宣大衡 劉家瑄

摘 要

本研究進行分析台灣西南海域BSR出現最集中地區之二垂直測線，在此地區來自中國大陸邊緣之快速沈積物可能有大量有機碳而形成為甲烷水合物之來源。

MCS 579-03測線向下穿過增積岩體，具有明顯之BSR現象，BSR上下沈積物之震測特徵受水深及構造特性之影響，剖面上BSR下方可發現多處具有強振幅、低頻率之現象，似與其下孔隙中可能存有游離天然氣有關。

MCS367-23位於增積岩體較高坡層軸部，詳細之速度分析顯示BSR之上地層之P波速度側向變化不明顯，其平均速度約1880m/s，而在BSR及其下地層之速度則有顯著差異，或與甲烷水合物、游離性天然氣、水之三相能組成有關，震波特性分析在日後有關甲烷水合物及其游離性天然氣之分析上將極有助益。

整體而言，BSR多出現在背斜頂部，逆衝構造及泥丘附近，由反射強度與瞬頻二者組合之特性有助於簡化並凸顯BSR現象，然而目前資料所能顯示者仍止於定性階段，欲進一步分析仍需較精確而完整之震測資料，此外，OBS資料中之水平分量將有助於了解S波速度、分析POISSON比進而並可使得AVO分析較為精確更具價值。

對於甲烷水合物之厚度及集中度分析極為重要，應為下一階段首需進行工作。